Improving lithographic masks with the assistance of indentations*

Guo Ying-Nan(郭英楠)[a)], Li Xu-Feng(李旭峰)[b)†], Pan Shi(潘 石)[a)‡], Wang Qiao(王 乔)[a)], Wang Shuo(王 硕)[a)], and Wu Yong-Kuan(吴永宽)[a)]

[a)] *School of Physics and Optoelectronic Technology, Dalian University of Technology, Dalian* 116024, *China*

[b)] *School of Applied Science, Taiyuan University of Science and Technology, Taiyuan* 030024, *China*

(Received 3 September 2011; revised manuscript received 31 October 2011)

Indentations etched on the output surface of a metallic mask are proposed to produce fine lithographic patterns with a resolution of 500 nm using the finite-difference time domain (FDTD) method. Such a designed mask is capable of enhancing near field lithography (NFL) resolution more than three times compared with the structure without indentations. The simulation results show that the interference disturbance between the adjacent lithographic channels can be eliminated efficiently by employing the indentations. As a straightforward consequence, the channel-to-channel interspaces can be shortened significantly, maintaining a uniform field distribution and high contrast.

Keywords: surface plasmons, lithography, finite-difference time domain (FDTD) method

PACS: 73.20.Mf, 42.82.Cr, 02.60.Cb **DOI:** 10.1088/1674-1056/21/5/057301

1. Introduction

With the rapid development of the microelectronics industry over the past several decades, the fabrication of nanoscale features is an urgent need and has been under intensive investigation. Among the prevailing lithographic methods, such as nanoimprinting lithography (NIL), dip-pen lithography (DPN), e-beam lithography (EBL) and focused ion-beam lithography (IBL),[1−5] photolithography has been the most widely used microfabrication technique due to its low cost, high throughput and ease of repetition. However, the diffraction limit is still a barrier in conventional photolithography with the highest resolution over half of the exposure wavelength. To improve the resolution, one straightforward method is to reduce the working wavelength to extreme ultraviolet light (EUV), soft X-rays or atomic wavepacket,[6−8] which drastically increases the complexity and cost for instrumentation and processing. As an improved photolithographic technique, near field lithography (NFL) has been proposed and demonstrated recently[9−16] based on the unique properties of surface plasmons (SPs), which are surface electromagnetic waves generated by the collective oscillation of electrons at the metal/dielectric interface.[17] Since SP modes may provide highly localized light signals in metallic nanostructures, much finer features with subwavelength resolution can be produced with a very large exposure wavelength. NFL can therefore go far beyond the free space diffraction limit. With the emergence of surface plasmon resonant interference nanolithographic techniques,[10] many subsequent investigations[12,13,16,18−20] on this subject have intensified, both theoretically and experimentally, in the transmission enhancement for apertures to improve signal contrast. This technique is suitable for fine small-area fabrication; when it comes to large-area fabrication, however, the shortcoming of interference lithography emerges for the restriction of the propagating distance of SPs (nearly 1.8 μm at Al/photoresist interface[12]) and it is hard to yield uniform lithography patterns.

Compared with interference nanolithography, Zeng *et al.*[14] made use of channel lithography with groove-array modification on the input surface, in which way the transmission can be increased 10 times compared with that of the bare slit.[21] An alternative method was put forward in our previous work,[15] by introducing a metallic nanostrip array right above the lithographic channels. With the assistance of the metallic nanostrip, more light can be coupled into the

*Project supported by the National Natural Science Foundation of China (Grant No. 10974025).

†Corresponding author. E-mail: xfli@mail.dlut.edu.cn

‡Corresponding author. E-mail: span@dlut.edu.cn

© 2012 Chinese Physical Society and IOP Publishing Ltd

lithographic channels, although it seems to block the incident light intuitively.[22] Both the methods mentioned above can produce a uniform field distribution with high contrast, but still have the drawback that the distance between the adjacent channels is at the micrometer scale due to the serious SP interference between them. Hence, further improvement in channel lithographic resolution is still required.

In this paper, we modify the model by etching indentations on the output surface to improve the lithographic resolution, and the resolution increases three times at the export of lithographic channels with large-intensity uniform field distribution as well as good contrast. The different contributions of the electric components are analysed and the phase distributions of the magnetic field are also illustrated and discussed.

2. Method and model

We employ a finite-difference time domain (FDTD) method,[23] and address a two-dimensional (2D) configuration, which is illustrated in Fig. 1. The NFL mask consists of a transparent glass as the substrate, and a silver nanostrip array lying right above the lithographic channels perforated into the silver layer, between which is a wafer as a support, and a protection layer of Cr with permittivity $\varepsilon_{\rm Cr} = -13.2436 + 14.616{\rm i}$[24] is adopted beneath the mask to inhibit the excitation of an unwanted surface wave mode. The bottom is a semi-infinite photoresist (PR) layer. The indentations, as the key part of our work, were etched at the export of the Cr surface to eliminate interference disturbance, and each of the indentations has width $w_{\rm s}$ and height $h_{\rm s}$. The periodicity Λ of the channels is set to be 500 nm. In contrast to our previous work, all the parameters not mentioned here are set to be the same as those in Ref. [15]. A plane wave of TM polarization (the magnetic field is perpendicular to the x–z plane; $|E_0| = 1$) with a wavelength of 436 nm impinges normally onto the top of the structure. The frequency dispersion of the silver complex permittivity is defined by the Drude model as

$$\varepsilon(\omega) = \varepsilon_0 - \omega_{\rm p}^2/[\omega(\omega + {\rm i}V_{\rm c})], \qquad (1)$$

where the vacuum permittivity $\varepsilon_0 = 4.9638$, plasma frequency $\omega_{\rm p} = 1.4497 \times 10^{16}$ rad/s and collision frequency $V_{\rm c} = 8.33689 \times 10^{13}$ rad/s were obtained from the best fit of the experimental values[25] over the visible wavelength range from 350 nm to 800 nm.[26] The mesh sizes are 2 nm × 2 nm in the x–z plane for better accuracy. Perfectly matched layers (PMLs) are used to avoid artificial reflections from the boundaries of the calculated domain.

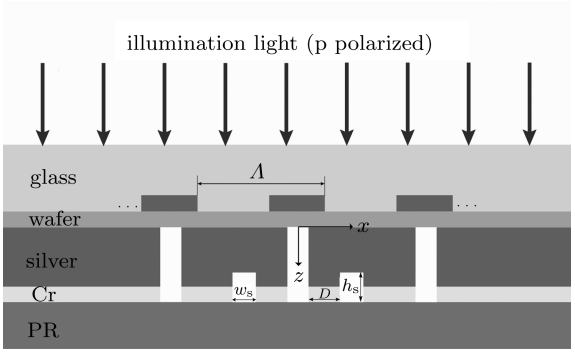


Fig. 1. Schematic representation of the proposed NFL mask, which consists of a silver film with a thickness of 230 nm, a Cr layer with a thickness of 20 nm lying below, three lithographic channels each with a width of 70 nm and a period of Λ perforated through both films, and the indentations etched between the adjacent channels, each with width $w_{\rm s}$ and depth $h_{\rm s}$. The interspacing distance between the indentation and the central channel is D. A silver nanostrip array with a width of 240 nm and a thickness of 44 nm lies right above the channels with a distance of 24 nm, and a wafer is introduced to support the nanostrip array with $n = 3$. The whole mask is attached to the glass with $n = 1.46$, and below the mask is a photoresist (PR) with $n = 1.53$. A normal incident TM polarized plane wave with a wavelength of 436 nm and a unit amplitude illuminates the mask.

3. Results and discussion

To better understand the interference mechanism, the electric field intensity of the three channel configurations without indentations are investigated first. A line monitor is set to be 50 nm away from the lithographic export to detect the electric field intensity distributions, which are given in Fig. 2 for $|E_{\rm tot}|^2 = |E_x|^2 + |E_z|^2$. One can see clearly that both the electric components E_x and E_z play different roles in the $E_{\rm tot}$ distributions. In Fig. 2(a), E_x shows a uniform field distribution with high intensity and is absolutely the main contributor to $|E_{\rm tot}|^2$ (Fig. 2(b)) at each channel export. While E_z is of opposite contribution; it reflects the coupling degree between the adjacent channels and has little influence on channel intensity enhancement. From our calculation, E_z becomes higher when the periodicity is shorter than 1.75 μm.[15] Thus, to enhance the E_x component and meanwhile depress E_z is an urgent target. For the given period $\Lambda = 500$ nm, two unwanted signals appear separately at the positions ($+x$ orientation, and

vice versa) of 186 nm and 324 nm, which are caused by the E_z component. In the following analysis, two point monitors are employed at such positions to detect the E_z intensity variation with indentation.

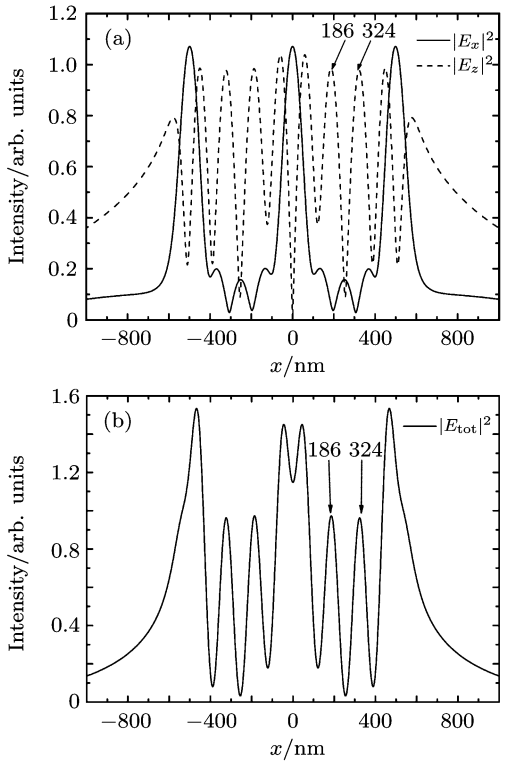


Fig. 2. Discrete electric intensity distributions of (a) $|E_x|^2$, $|E_z|^2$ and (b) $|E_{\rm tot}|^2$ with $\Lambda = 500$ nm for no introduced indentations.

We take the indentations into consideration, ignore the position influence which will be discussed later, and set the indentations to be in the middle of the adjacent channels with the height fixed at 50 nm. The underlying physics behind the magic indentations is the phase variation at the output interface, which is in contrast to that in the case without indentations. In Fig. 3(a), the E_z intensity shows a quadratic-like dependence on the indentation width. The presence of the indentations at the output interface provides an effective refractive index ($n_{\rm eff}$), which changes the phase of the SP wave. After propagating through the indentation, the SP wave experiences phase retardation ($\sim \beta h_{\rm s}$); herein, β is the propagation constant and follows the formula[27]

$$\tanh\left(\sqrt{\beta^2 - k_0^2\varepsilon_{\rm d}}\,w_{\rm s}/2\right) = -\varepsilon_{\rm d}\sqrt{\beta^2 - k_0^2\varepsilon_{\rm m}}\Big/\left(\varepsilon_{\rm m}\sqrt{\beta^2 - k_0^2\varepsilon_{\rm d}}\right), \quad (2)$$

where $\varepsilon_{\rm d}$ and $\varepsilon_{\rm m}$ are, respectively, the permittivities of the dielectric and the metal, $k_0 = 2\pi/\lambda_0$ is the free-space wave vector, and β is the propagation constant represented as the effective index $n_{\rm eff} = \beta/k_0$ of the waveguide for SPs. In this formula, the effective index shows an exponential attenuation with the increase in $w_{\rm s}$, which could be found easily from Fig. 3(b). Thus,

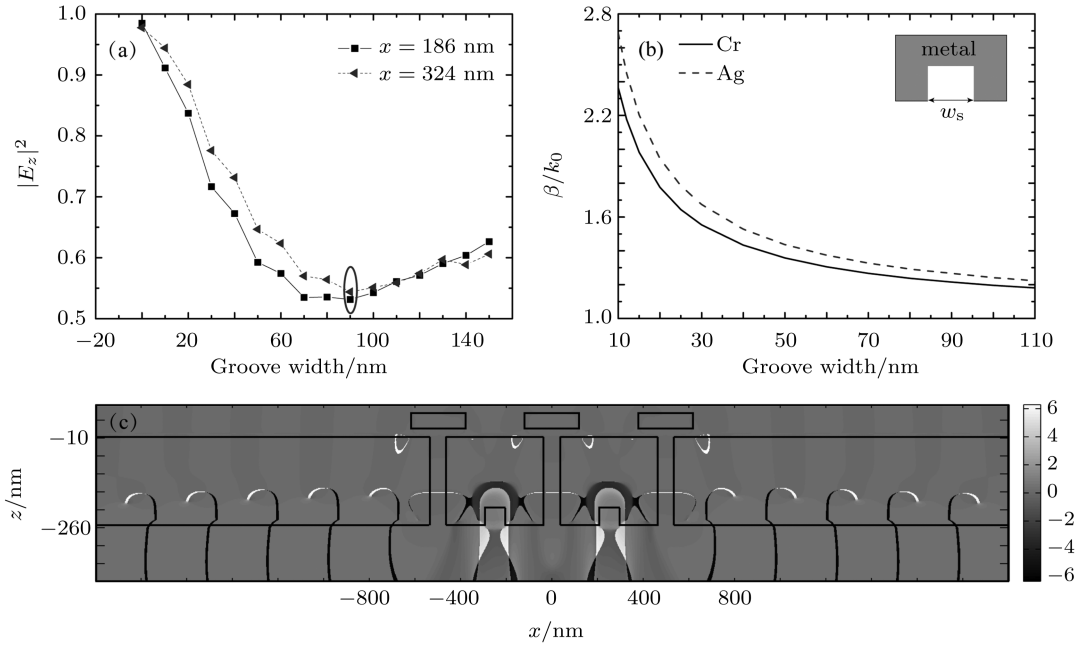


Fig. 3. (a) Variations in the field intensity of the E_z component with indentation width $w_{\rm s}$ at positions $x = 186$ nm and $x = 324$ nm. (b) Curves for the effective index $n_{\rm eff} = \beta/k_0$ of the indentation versus its width for Cr (solid line) and Ag (dashed line) metals. (c) The difference in the phase of the H_y component between the configuration with indentations ($h_{\rm s} = 50$ nm, $w_{\rm s} = 90$ nm) and without indentations (unit: rad).

there must be an optimal width to satisfy the phase matching and then form destructive interference. In our configuration, an optimal indentation width of 90 nm is obtained for a given indentation height of 50 nm (denoted by a circle). The difference in the phase of the magnetic component (H_y) between the configurations with/without indentations ($h_s = 50$ nm and $w_s = 90$ nm) is given in Fig. 3(c). The phase distributions show that at the export of the indentations, the phase of H_y is almost changed by π. This can be explained as follows: the SP wave propagating from the channel splits into two parts, i.e., one goes directly along the output surface and the other goes via the indentations, and then the two waves converge together with converse phase, and consequently the unwanted disturbance signals are eliminated.

Figure 4(a) shows the variance in the values of E_z intensity with the increase in indentation height at the $x = 186$ nm and $x = 324$ nm positions, fixing the indentation width to be 90 nm. Both curves exhibit a periodic oscillation that has already been discussed in Refs. [14] and [21] using Fabry–Perot (F–P) resonance condition

$$2k_0\mathrm{Re}(n'_{\mathrm{eff}})h_s + \arg(\rho_1\rho_2) = 2m\pi, \tag{3}$$

where m is an integer, n'_{eff} is the effective index of indentation, and $\arg(\rho_1\rho_2)$ denotes the phase of the reflected SP wave at the upper and lower interfaces of the indentations. By appropriately choosing the indentation height to fulfill the F–P resonance condition, the constructive or destructive interference will be provided. For the constraint of the film thickness in this work, only one periodicity of 170 nm appears in Fig. 4(a), and it matches well with the theoretical value calculated by Eq. (3), i.e. $\lambda/2n_{\mathrm{eff}} \approx 179$ nm. Herein, the optimal indentation depth is obtained at 50 nm (denoted by a circle). Figures 4(b) and 4(c) show the profiles of field intensity $|E_{\mathrm{tot}}|^2$ without/with indentations etched at the output interface, respectively. Comparing Fig. 4(b) with Fig. 4(c), we can obviously see that the interference pattern in Fig. 4(b) is eliminated, so the vivid signals in the channel export can be easily detected with high contrast.

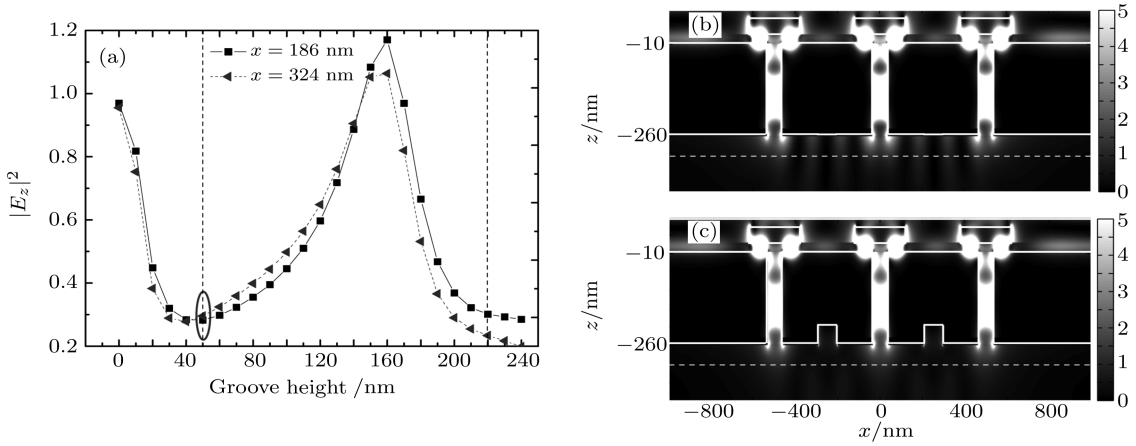


Fig. 4. (a) Variations in the field intensity of the E_z component with indentation height h_s at the $x = 186$ nm and $x = 324$ nm positions. The profiles of field intensity $|E_{\mathrm{tot}}|^2$ without indentations and with etched indentations are shown in panels (b) and (c), respectively. The indentation parameters are set to be $h_s = 50$ nm and $w_s = 90$ nm in the centre of the adjacent channels.

From this point onwards we consider an interesting special case of the best indentation position for E_z component modulation. With the indentation parameters fixed to be $h_s = 50$ nm and $w_s = 90$ nm, Fig. 5(a) depicts the variations in total field intensity at positions $x = 186$ nm and $x = 324$ nm with channel-to-indentation interspace D, showing a periodic variation of 140 nm $\approx \lambda_{\mathrm{sp}}/2$, where $\lambda_{\mathrm{sp}} = \lambda_0\sqrt{(\varepsilon_m + \varepsilon_d)/\varepsilon_m\varepsilon_d} = 258.56$ nm ≈ 260 nm at the Cr/PR interference. Because the positions of the two interference peaks at different D values shift slightly, the relative intensities of both recording spots do not match very well, which does not influence our conclusions. From our calculation, three optimal positions $D = 170$ nm (the centre), 30 nm and 310 nm are found and denoted by circles, and their field intensities on the output surface are given in Figs. 5(b), 5(c) and 5(d), respectively. Three uniform field intensity distributions with high contrast can be obtained, from which one can easily find the magic effect of the indentations in the removal of interference disturbance. Additionally, the symmetrical side-etchings of $D = 30$ nm and 310 nm exhibit a much higher contrast than the central-etching.

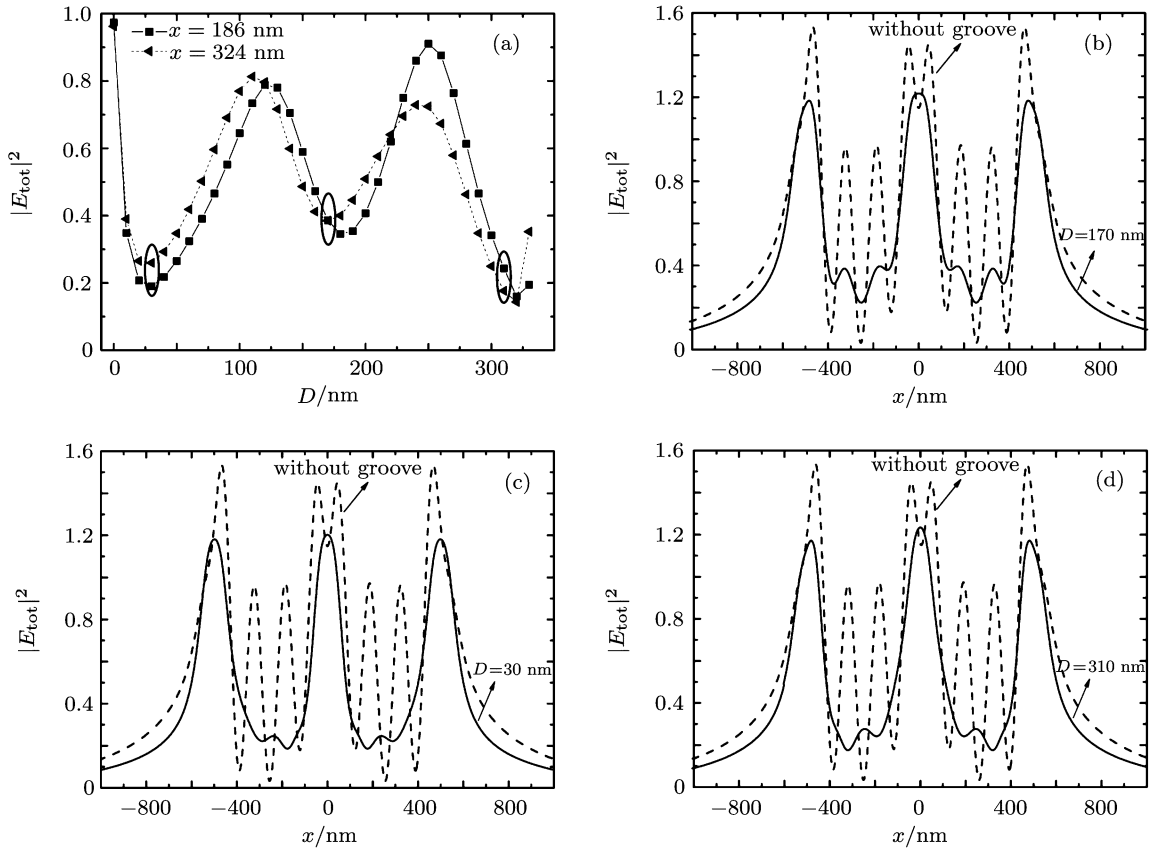


Fig. 5. (a) Variations in field intensity with the interspace between the indentation and central channel D at the $x = 186$ nm and $x = 324$ nm positions. Panels (b), (c) and (d) show the variations in field intensity with D in the centre ($D = 170$ nm), and at the symmetrical sides $D = 30$ nm, $D = 310$ nm, respectively.

Finally, we estimate the influence of periodicity on field intensity in the case without indentation. A point monitor is set to be 50 nm below the export of the central channel; the intensity variation with period is depicted in Fig. 6. The damped oscillation curve shows a period of 260 nm, which is the same as the SP wavelength. When the channel periodicity Λ is short (see the first peak), almost equal to the length of the metallic nanostrip (240 nm in this work), the interspaces between the nanostrips are so small that not enough light converges into the channel. As a straightforward consequence, a very tiny field intensity is detected at the channel export. With the Λ increasing, more light is coupled into the channel, thereby enhancing the channel-to-channel coupling effect simultaneously, thus the field intensity is enhanced to 1.6. Further increasing Λ will weaken the channel coupling, so that the export intensity is decaying oscillation at a value of 1. From the periodicity analysis, we can optimize the metal film and the nanostrip parameters to design masks with a much higher resolution.

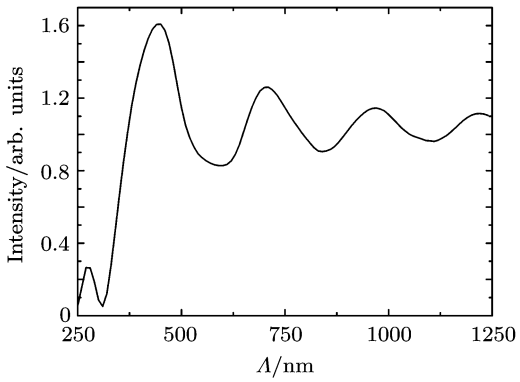


Fig. 6. Field intensity versus mask periodicity Λ at the test point 50 nm away from the export of the central channel.

4. Conclusions

An improved NFL mask with indentations etched onto the output surface is proposed to enhance NFL resolution more than three times compared with the structure without indentations. Numerical analysis demonstrates that the two electric components have

different contributions to the field enhancement. E_x is the main contributor to the field intensity at channel export, while the E_z component contributes to the channel-to-channel interference disturbance. The presence of indentations changes the phase of the surface plasmon waves at the output interface, and thus the indentation with optimal parameters could eliminate the inference disturbance efficiently. The indentation position also shows a periodic variation in $\lambda_{\rm sp}/2$, and the bilateral etching is better than the central etching. Such a lithographic method is able to shorten the channel-to-channel distance with only one single indentation in between, and has the potential to realize high-resolution large-area lithography.

References

[1] Chou S Y, Krauss P R and Renstrom P J 1996 *Science* **272** 85

[2] Bailey T, Choi B, Colburn M, Meissl M, Shaya S, Ekerdt J, Sreenivasan S and Willson C 2000 *J. Vac. Sci. Technol.* B **18** 3572

[3] Piner R D, Zhu J, Xu F, Hong S and Mirkin C A 1999 *Science* **283** 661

[4] Tseng A A, Chen K, Chen C D and Ma K J 2003 *Electronics Packaging Manufacturing, IEEE Transactions on* **26** 141

[5] Melngailis J, Mondelli A, Berry III I L and Mohondro R 1998 *J. Vac. Sci. Technol.* B **16** 927

[6] Gwyn C, Stulen R, Sweeney D and Attwood D 1998 *J. Vac. Sci. Technol.* B **16** 3142

[7] Silverman J P 1998 *J. Vac. Sci. Technol.* B **16** 3137

[8] Johnson K S, Thywissen J H, Dekker N H, Berggren K K, Chu A P, Younkin R and Prentiss M 1998 *Science* **280** 1583

[9] Srituravanich W, Fang N, Sun C, Luo Q and Zhang X 2004 *Nano Lett.* **4** 1085

[10] Luo X and Ishihara T 2004 *Appl. Phys. Lett.* **84** 4780

[11] Luo X and Ishihara T 2004 *Opt. Express* **12** 3055

[12] Liu Z, Wei Q and Zhang X 2005 *Nano Lett.* **5** 957

[13] Xu T, Fang L, Zeng B, Liu Y, Wang C, Feng Q and Luo X 2009 *J. Opt.* **11** 085003

[14] Zeng B, Pan L, Liu L, Fang L, Wang C and Luo X 2009 *J. Opt.* **11** 125003

[15] Li X, Pan S, Wang Q, Guo Y and Wu S 2010 *J. Opt.* **12** 115504

[16] Ge W, Wang C, Xue Y, Cao B, Zhang B and Xu K 2011 *Opt. Express* **19** 6714

[17] Raether H 1988 *Surface Plasmons on Smooth and Rough Surfaces and on Gratings* (Berlin: Springer-Verlag) p. 136

[18] Liu Z, Wang Y, Yao J, Lee H, Srituravanich W and Zhang X 2008 *Nano Lett.* **9** 462

[19] Yin Y, Li T, Xu P, Jin H and Zhu S 2011 *Appl. Phys. Lett.* **98** 093105

[20] Li H H, Chen J and Wang Q K 2010 *Chin. Phys.* B **19** 114203

[21] Li Z, Yang Y, Kong X, Zhou W and Tian J 2009 *J. Opt.* **11** 105002

[22] Cui Y and He S 2009 *Opt. Lett.* **34** 16

[23] Taflove A and Hagness S C 1995 *Computational Electrodynamics: the Finite-Difference Time-domain Method* (Boston: Artech House) Vol. 347

[24] Palik E D 1985 *Handbook of Optical Constants of Solids* (New York: Academic Press) p. 547

[25] Johnson P and Christy R 1972 *Phys. Rev.* B **6** 4370

[26] Kawata S, Ono A and Verma P 2008 *Nature Photonics* **2** 438

[27] Gordon R and Brolo A 2005 *Opt. Express* **13** 1933